# Stochastic Resonance Emergence from a Minimalistic Behavioral Rule

Shuhei Ikemoto[a], Fabio DallaLibera[b,c], Hiroshi Ishiguro[b,d]

[a]*Department of Multimedia Engineering, Graduate School of Information Science and Technology, Osaka University, 2-1 Yamada-oka, Suita, Osaka, Japan*
[b]*Asada Project, ERATO, Japan Science and Technology Agency, Osaka University, 2-1 Yamada-oka, Suita, Osaka, Japan*
[c]*Department of Information Engineering (DEI), Faculty of Engineering, Padua University, Via Gradenigo 6/a, Padua, Italy*
[d]*Department of Systems Innovation, Graduate School of Engineering Science, Osaka University, 1-3 Machikaneyama, Toyonaka, Osaka, Japan*

**Abstract**

Stochastic resonance (SR) is a phenomenon occurring in nonlinear systems by which the ability to process information, for instance the detection of weak signals is statistically enhanced by a non-zero level of noise. SR effects have been observed in a great variety of systems, comprising electronic circuits, optical devices, chemical reactions and neurons. In this paper we report the SR phenomena occurring in the execution of an extremely simple behavioral rule inspired from bacteria chemotaxis. The phenomena are quantitatively analyzed by using Markov chain models and Monte Carlo simulations.

*Keywords:* Stochastic resonance, chemotaxis, control

## 1. Introduction

Stochastic resonance (SR)[1][2] is a phenomenon for which the addition of random noise can enhance the response to weak inputs in nonlinear systems. Originally, SR was proposed by Benzi et al. to explain the periodic recurrence of ice ages[1], the so-called Milankovitch cycles. In detail, the Earth climate supports two stable states, one at a lower temperature (an ice age) and one at a higher temperature. The external small, periodic modulations of the Earth orbit were modeled as a deterministic "input" that biases the random climate changes toward one of the two states. Fluctuations attributable to the

interactions between the atmosphere, the hydrosphere, the cryosphere and the lithosphere were modeled as "random noise" that can cause transitions between those two stable states. If the fluctuation amplitude is excessively small, then the transitions occur too infrequently and out of tune with the modulation given by the Earth orbit. Conversely, if the fluctuations are excessively large, the random transitions would be too frequent and, therefore, not correspond to the modulation of the Earth orbit. However, for an optimal amplitude of the fluctuations driven by the random noise, the transitions can exhibit the period given by the small periodic modulation of the Earth.

Since its appearance in the seminal paper of Benzi et al., SR has been attracting a lot of interest, and is being intensively studied. SR effects were shown in a great variety of systems [3, 4]. In [5] Fauve and Heslot reported a stochastic resonance effects in a discrete two-state electronic Schmitt trigger. Successively, McNamara et al. [6] identified a SR effect in an optical bistable system, a bidirectional ring laser. Several studies report SR effects in semiconductors [7, 8], as well as in chemical reactions [9, 10, 11].

Stochastic resonance has been observed also in systems that do not include energetic barriers or sensing threshold, as shown in [12] using a model in which a sequence of pulses is generated randomly with a probability function of the input.

Several examples where technological applications could benefit from the SR effect were presented, for instance [13] reports experiments on the response of a superconducting loop with a Josephson-junction barriers, the central element of a radio frequency Superconducting QUantum Interference Device (SQUID). Similarly, [14] shows that the sensing of nonlinear optomechanical oscillators can be enhanced by SR effects. Interestingly, in [15] Collins at all. showed that the range of noise amplitudes for which SR occurs can be very wide.

SR appears to be exploited by living beings as well. For example, SR effects were reported in ion channels [16], sensory neurons [17, 18], neuronal networks of mammalian brains [19], and physiological systems [20, 21]. Stochastic resonance phenomena can also be observed at a behavioral level, for instance in the synchronization of the cell dynamics due to extracellular noise [22], detection of plankton by the paddle-fish [23] or in human posture stabilization [24] and attention control [25].

One of the simplest behaviors found in nature is *chemotaxis*, the process by which bacteria [26, 27, 28] or eukaryotic cells [29, 30, 31, 32, 33] sense chemical gradients and move with directional preference toward food sources.

In this paper we aim at showing that also this primitive and essential behavior found in bacteria could be exploiting SR.

Among the most thoroughly studied organisms with regards to chemotaxis we can certainly cite Escherichia coli (E. coli), often taken in consideration due to its well-characterized physiology, its simple chemotaxis signaling pathway, its capacity to sense small concentration gradients of a chemoattractants, and its possible use as either a natural host or a surrogate host for plasmids coding of desired features or products [34].

This bacterium has only two ways of moving, rotating clockwise or counterclockwise [26]. When it rotates counter-clockwise, the rotation aligns its flagella into a single rotating bundle and it swims in a straight line. Conversely, clockwise rotations break the flagella bundle apart and the bacterium tumbles in place. The bacterium keeps alternating clockwise and counterclockwise rotations. In absence of chemical gradients, the length of the straight line paths, generated by counter-clockwise rotations, is independent of the direction. As a consequence, the movement consists in a random walk. In case of a positive gradient of attractants, like food, E. coli reduces the tumbling frequency. In other terms, when the concentration of nutrients increases, the bacterium proceeds in the same direction for a longer time. This strategy allows to bias the overall movement toward increasing concentrations of the attractant. Such a simple mechanism works despite the difficulties in precisely sensing the gradient. Actually, the spatial gradients in concentration cannot be sensed directly due to the small dimensions of the bacteria, so temporal difference in the concentration is used to estimate the nutrient distribution.

A wide spectrum of models, from a very abstract point of view to the modeling of the protein interactions, is available in literature [35, 36, 37].

Few studies however analyze the effect of noise on the chemotactic behavior. Furthermore, the noise is seen mainly as a nuisance in sensing that should be filtered out by the bacterium [38, 34], similarly to what is usually done in control theory.

Using a very general model, we instead show that external noise can actually increase the chemotactic performance. Precisely, we show that the presence of an appropriate level of noise can increase the mutual information between the stochastic distribution of the position of bacteria performing chemotaxis and the spatial concentration of nutrients. This mutual information increase corresponds to an increase of the chemotactic performances, revealing that external (or internally generated) noise can actually be bene-

ficial for chemotactic behaviors.

## 2. Minimalistic behavioral rule

Living beings are very interesting from an engineering point of view, since while robots find difficulties in coping with noise and errors in the recognition or control processes [39, 40, 41], biomolecules [42] operate using energies comparable to thermal fluctuations. Chemotaxis is one of these cases where the mechanism adopted by living organisms reveals to be a simple solution for the control of robots as well [43, 44, 45].

We found that the following simple behavioral rule can work appropriately for a large variety of problems:

- when the current behavior works well, the following behavior is generated by applying random fluctuations to the current behavior
- when the current behavior does not lead to improvements of the robot state, the following behavior is chosen randomly.

The previous rule can be formalized mathematically in a way independent from the problem setup. Let us define with the generic term "particle" a robot, a simulated bacteria, or any agent moving according to the rule. Denote by $\boldsymbol{x}_t \in \mathbb{R}^n$ its state at time $t$ and similarly by $\boldsymbol{u}_t \in \mathbb{R}^m$ the action taken by the particle at time $t$. We do not assume any particular constraint in the problem setup or in the meaning of each of the components of $\boldsymbol{u}_t$. As a very simple example, however, we could imagine to have a particle moving on a plane, and to denote by $\boldsymbol{x}_t \in \mathbb{R}^2$ its position at time $t$. The motor command $\boldsymbol{u}_t \in \mathbb{R}^2$ could represent the movement that the particle makes during the $t$-th time step. In this case, the effect of the motor command would simply be $\boldsymbol{x}_{t+1} = \boldsymbol{x}_t + \boldsymbol{u}_t$. In general, we have that the state of the particle at time $t+1$ is a function of $\boldsymbol{x}_t$ and $\boldsymbol{u}_t$, i.e. $\boldsymbol{x}_{t+1} = f(\boldsymbol{x}_t, \boldsymbol{u}_t)$.

The behavioral rule we propose can be formalized in a straightforward manner in a completely general way as well. Denoting by $u_t^i$ the $i$-th component of the motor command at time $t$, the same component at time $t+1$ is given by:

$$u_{t+1}^i = \begin{cases} u_t^i + \eta^i R & if\ \Delta A_t \geq 0 \\ random\ selection & otherwise \end{cases} . \tag{1}$$

Where $R \sim \mathcal{N}(0,1)$ is a random variable and $\Delta A_t$ expresses how much the particle improved its state during the $t$-th timestep. For instance, in a goal reaching setup, $\Delta A_t$ could express how much the particle got closer to its target. In the case of a living organism, $\Delta A_t$ could represent the variation in the concentration of nutrients.

Some examples of the emergent behavior of a particle that tries to reach a goal following the rule are reported in Fig. 1. In the first panel, the initial direction is quite skewed compared to the optimal direction. Thanks to the random perturbations, by the third step the direction is identified as a bad direction and a new heading is chosen at random. The second panel shows a case in which the initial direction is bad, and a good direction is found only after changing the direction randomly three times. In the third panel, the initial direction is strongly skewed compared to the optimal one, and it is identified as a bad direction by the second step. The newly chosen direction is quite skewed as well, and identified as such by the seventh step. At this point, a good direction is chosen and kept (with small perturbation) until the last step. Intuitively, the random perturbations "increase the sensitivity" of the particle, by letting it identify strongly skewed directions, even if it only receives a binary information telling whether during the last time step it got closer to the goal or not.

Actually, by using this extremely simple behavioral rule, behavior changes are controlled only by modulating the level of random perturbations. In particular, using solely the binary information given by the sign of $\Delta A$, the control algorithm either applies a small perturbation that leads to a SR effect or changes the motor command in a completely stochastic manner.

If no perturbations are introduced ($\eta^i = 0$), then the binary evaluation can only correspond directly to "keeping" or "changing" the motor command $\boldsymbol{u}_t$. In such a case, the time-series profile of $\boldsymbol{u}_t$ will consist in a series of abrupt command changes followed by periods in which the motor command is kept constant. This kind of behavior can be inefficient since the same motor command can be kept for a long time even if the improvement to the particle conditions (e.g. the decrease in the distance to the goal, increase of the nutrient concentration, etc.) is very limited. Conversely, large perturbation levels can make the behavior of Eq. 1 very close to a random walk, giving in general very poor performances. Intuitively, therefore, there exists an opportune level of random perturbations in the between, for which on the one hand the probability of keeping using inefficient motor commands is decreased and on the other hand the frequency by which a new motor command is

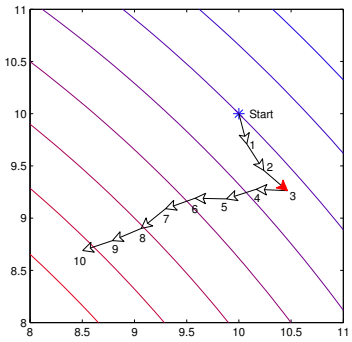


(a)

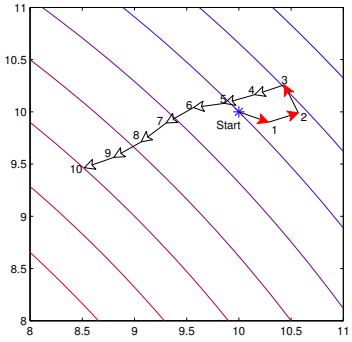


(b)

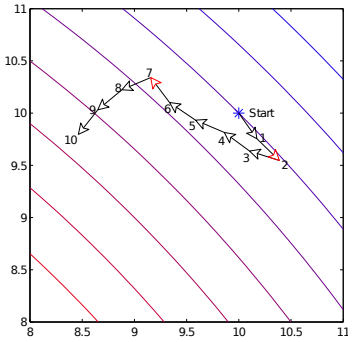


(c)

Figure 1: Examples of trajectories taken by a particle moving according to the rule presented. The particle is initially located in $[10, 10]^T$, and takes 10 steps of length 1, aiming at a goal (not displayed) located in $[0, 0]^T$. When the particle got closer to the goal (white arrow), a small perturbation was added to the particle direction. When the particle got further from the goal (filled arrow), a new random direction was taken. Points at the same distance from the goal (contour lines) are shown for clarity.

selected is not excessive. Figure 2 reports a concrete example. The position of a particle $\boldsymbol{x}_t$ is initially set to $\boldsymbol{x}_t = [1, 1]^T$ and updated by $\boldsymbol{x}_{t+1} = \boldsymbol{x}_t + s \cdot [cos(u_t), sin(u_t)]^T$, $\boldsymbol{u}_t \in \mathbb{R}$, $\boldsymbol{x}_t \in \mathbb{R}^2$, $t \in \mathbb{N}$, $s = 10^{-3}$, where $u_t$ is determined by our simple behavioral rule and $\Delta A_t$ expresses how much the robot got closer to the goal. In practice, this setup could correspond to the movement of a holonomic robot, i.e. a robot that can move in any direction thanks to an opportune configuration of the wheels.

The top panel reports the average distance traveled toward the goal in $10^3$ steps for different values of $\eta$. We notice that the curve assumes the typical shape of a SR effect.

In this paper the behavioral rule inspired by bacteria chemotaxis reported in Eq. 1 will be analyzed by simple statistical models. In particular, section 3.1 will show how the performance increase obtained for an appropriate random perturbation $\eta$ can be explained by a change in the distribution of the directions taken by the particle.

Section 3.2 will report an analysis of the behavior of a particle that moves according to the rule in simple continuous scalar potential fields $A(\boldsymbol{x})$, which could represent the food concentration for a bacteria or an artificial potential field for a robot. It will be shown that the expected value of the movement orientation is equal to the steepest gradient at each time step, although from Eq. 1 it is clear that the algorithm considers only the sign of $\Delta A_t = A(\boldsymbol{x}_t) - A(\boldsymbol{x}_{t-1})$, i.e. it takes as input solely a binary information expressing whether in the previous time step the particle improved its state or not.

Section 4 will present the results of Monte Carlo simulations of particles that move on a potential field $A(\boldsymbol{x})$ controlled by Eq. 1. We compute the mutual information between the potential field $A(\boldsymbol{x})$ and the spatial distribution of the particles, and show that the mutual information can be maximized with appropriate levels of $\eta$.

Finally, section 5 will summarize the paper and highlight future research directions.

## 3. Markov Model trajectory simulation

In this section we will present the Markov chain models for the movement of a particle over simple potential fields. In particular, we will analyze the direction taken by a particle moving in a two dimensional plane in two cases. The first case involves a linear potential field that increases along the horizontal axis and assumes the same value over the vertical axis. In the second

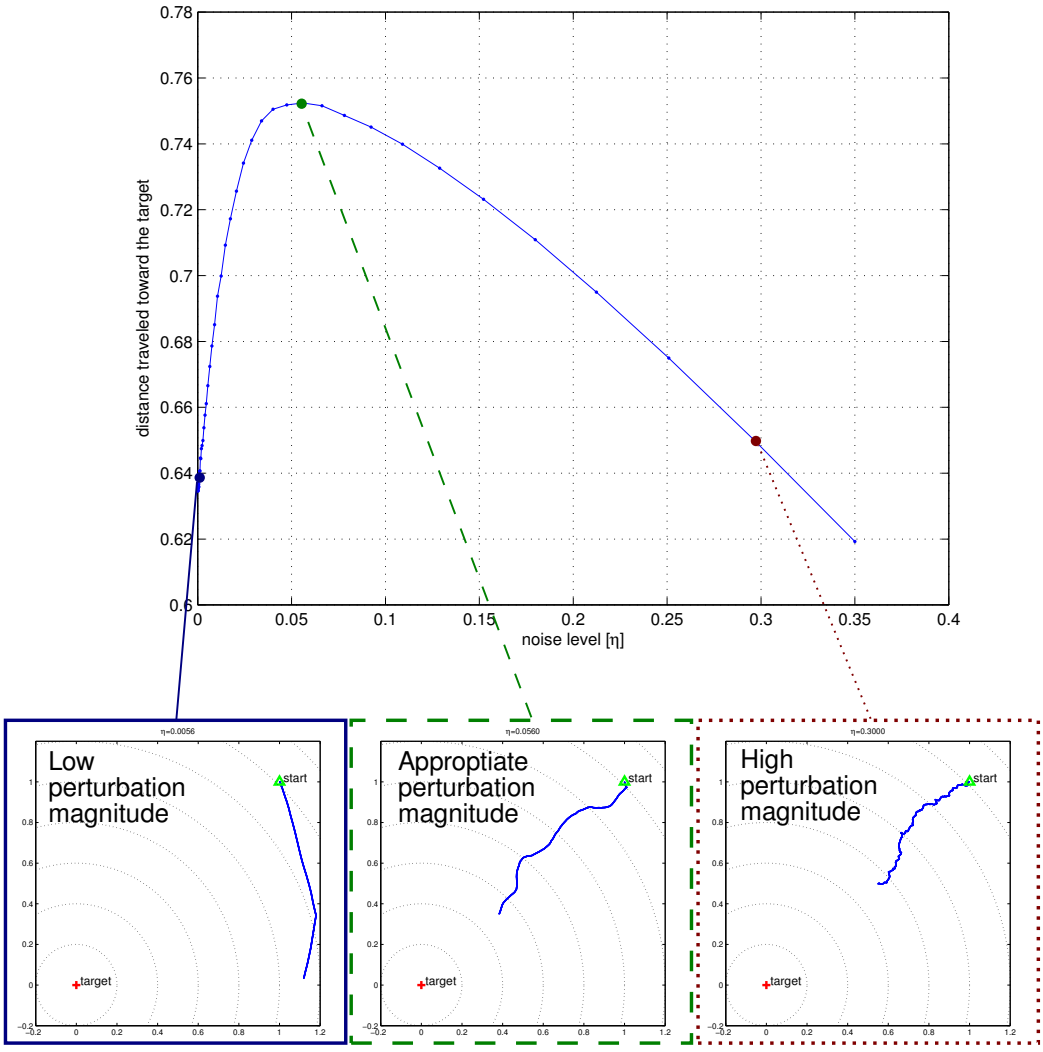


Figure 2: Performance for different perturbation magnitudes. The top panel reports the performances for different values of $\eta$. The performance is measured as the distance traveled toward the goal in $10^3$ time steps, averaged over $10^6$ simulations. The bottom panels report examples of trajectories obtained for different values of $\eta$. Precisely, the first trajectory was obtained for a low perturbation level, $\eta = 0.0056$, the second trajectory corresponds to an opportune level of perturbation, $\eta = 0.56$ and finally the bottom right panel reports a trajectory generated with $\eta = 0.3$.

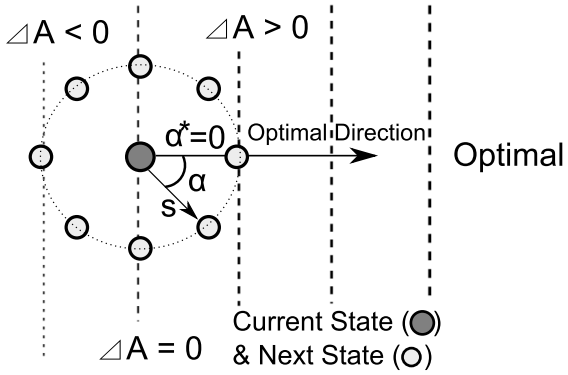


Figure 3: The schematic representation of the Markov model used to investigate the probability of the directions taken on a linearly increasing potential field. The model represents a particle that moves on a ramp-shaped potential field by taking steps of constant length $s$ with angle $\alpha$ to the horizontal (optimal) direction. The $N$ states represent the directions taken and can be assumed to be located equally spaced on a circle centered at the current particle position.

case, the potential field is given by a Gaussian centered in the origin, i.e.

$$A(\boldsymbol{x}) \;\; = \;\; \exp\left\{-\boldsymbol{x}^T \Sigma \boldsymbol{x}\right\} \tag{2}$$

where $\Sigma$ is a positive definite matrix. We analyze the behavior for two different $\Sigma$ matrices, and show that in both cases the average trajectory corresponds to the steepest gradient.

*3.1. Ramp shaped potential field model*

In order to test the direction taken by a particle that moves according to Eq. 1, let us derive a Markov model that describes the case of a particle moving over a potential field shaped as a ramp, i.e. a potential field that increases linearly along the horizontal axis and assumes the same value along the vertical axis, $A(\boldsymbol{x}) = x_1$.

Fig.3 provides an illustration of the Markov model.

The direction that the particle can assume is discretized in a set of $N$ possible states, ideally located on a circle centered at the particle position. Each state $j$ can therefore be imagined to be associated to the vector $\boldsymbol{x}^{(j)} = [\cos(2\pi j/N)\ \ \sin(2\pi j/N)]^T$, $0 \leq j < N$.

The states can be divided in two groups, $S^-$ and $S^+$, respectively one corresponding to the states with a lower potential value (the ones ideally on

the "left" of the current position, i.e. having $\boldsymbol{x}_1^{(j)}$ positive) and the other corresponding to the states representing points with a higher or equal potential value. According to Eq. 1, when the potential increases, the next state is obtained as a perturbation of the current state. When the potential decreases, the state is chosen completely randomly. The transition probability $P(i,j)$ between a state $i$ and a state $j$ was therefore set as

$$P(i,j) = \begin{cases} 1/N & if\ i \in S^- \\ \int_{2\pi(j-i)/N-\pi/N}^{2\pi(j-i)/N+\pi/N} f(\theta)d\theta & if\ i \in S^+ \end{cases}. \tag{3}$$

where $f(\theta)$ is the Von Mises distribution centered in 0 ($\mu = 0$). The stationary distributions for $N = 100$ and for several values of the concentration parameter $\kappa$ ($\kappa = 1/\eta^2$) of the Van Mises distribution were calculated.

Remembering that the states represent different directions and that therefore their stationary probability actually approximates the probability density function of the various directions, it is possible to define the performance obtained for a certain value of $\eta$ as $\sum_{j=0}^{N-1} P(j)x_1^{(j)}$, i.e. as the expected value of the potential value increase. The first panel of Fig. 4 shows the performance for different perturbation levels $\eta$. We notice that the performance is always positive, i.e. despite its simplicity, the behavioral rule of Eq. 1 is able to bring the particles to increasing potential values. More interestingly, it is possible to observe a typical SR effect, with the performance increasing as long as the perturbation is increased until a peak is reached for $\eta \approx 0.04$, after which increasing the perturbation level causes a performance decrease.

Observing the stationary distributions in detail, it is possible to have a better idea of the actual reason of the performance increase and the subsequent decrease when increasing the value of $\eta$. Expressly, for very low values of $\eta$, the distribution of the directions taken is approximately uniform, i.e. the probability assumes essentially the same value for all the states in $S^+$ and 0 for the states in $S^-$. The distribution becomes more and more peaky, with the peak centered at the optimal direction, when the value of $\eta$ is increased until its optimal value, as shown in the second panel of Fig. 4. After reaching this point, increasing the perturbation level makes the distribution mass spreads over all the states, including the ones in $S^-$, with a consequent decrease of the probability of the states in $S^+$. As explained informally in the introduction and reported in Fig. 2, the model shows quantitatively that actually

- for low values of $\eta$, the probability of directions with low, positive performance is high.
- for an appropriate level of $\eta$, the probabilities of choosing suboptimal directions is decreased in favor of directions that lead to higher performances.
- an excessive perturbation level spreads the probability over all the directions, including the ones with low performance.

Observing the probability densities obtained, it is easy to see that the probability distribution shapes are different for $\eta$ values smaller or higher than the optimal value. This provides an intuitive reason for the asymmetry of the performance curve reported in Fig. 4(a).

Direct inspection of the transition probabilities also provides insights on the mechanism underlying the SR effect observed in the execution of the behavioral rule specified by Eq 1. In particular, observing the transition probabilities among states in $S^+$ that lead to small potential value increases and states in $S^-$ that lead to small potential value decreases, it results that the transition probabilities from states in $S^+$ to states in $S^-$ are higher than the probabilities of the opposite transitions from states in $S^-$ to states in $S^+$. In other terms, the model suggests that with optimal values of $\eta$ it is easy to detect and leave states with low performance thanks to the transition to states in $S^-$ but it is difficult to enter those low performance states.

This observation allows us to derive further considerations. The behavioral rule in Eq. 1 imposes choosing the next motor command (direction) completely randomly as soon as the potential field value decreases, even slightly. This may appear as a too simple rule, and better performances would be expected by modulation of the perturbation level, with higher perturbations levels for stronger potential decreases. However, such smooth transitions would prevent the beneficial asymmetry of the transition probabilities described here, with a consequent performance decrease, as can be readily shown with Monte Carlo simulations.

### *3.2. Gaussian shaped potential field model*

In order to model a setting closer to the bacteria chemotaxis or robot task reaching, let us consider a particle that moves in a two-dimensional plane, where a Gaussian shaped potential field is defined. This potential field could represent, for instance, the concentration of a certain nutrient at

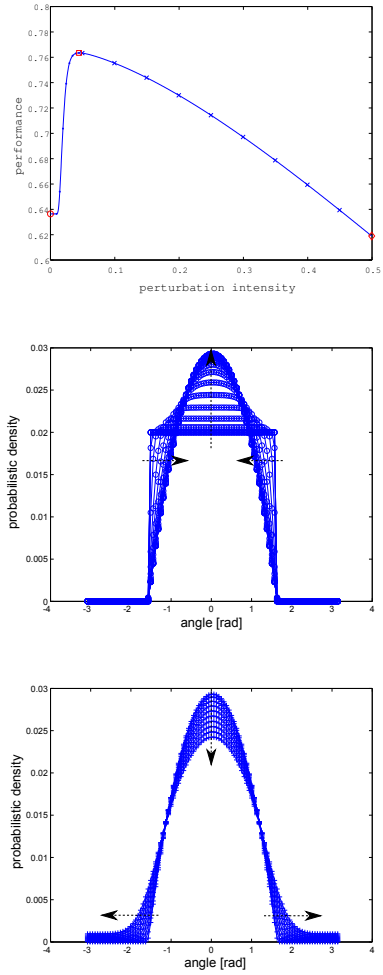


Figure 4: Results for the linearly increasing potential field. The first panel presents the relationship between the size of noise $\eta$ and the performance, defined as the expected value of the potential field value increase. The second and third panel show several stationary distributions for different noise sizes $\eta$. In particular, the second panel shows distributions with a perturbation level lower than the optimal. The distributions become more and more concentrated to states with high performance (small deviations from the optimal angle) as the perturbation level gets closer to the optimal value. The third panel shows the stationary distributions for values of $\eta$ higher than the optimal. By increasing the value of $\eta$, the stationary distribution probability is spreads more and more among the states. This decreases the bias toward the states with high performances, that is obtained for appropriate (lower) perturbation levels.

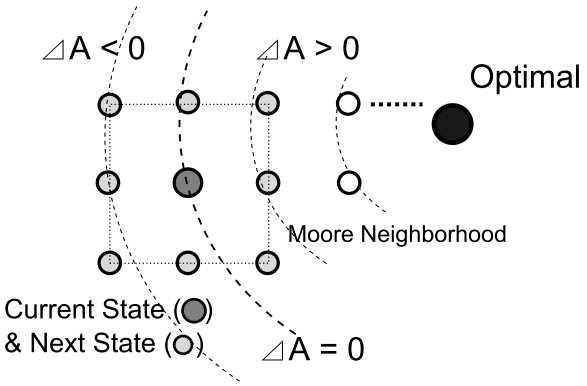


Figure 5: Schema of the Markov Model used to investigate the trajectories of the particles over a Gaussian field. The states are imagined to be placed over a grid and the movement of the particles is approximated by a second order Markov Model. Since the behavior depends on whether the value of the potential field increased in the previous step or not, a second order Markov Model is used.

every point of the plane, with the peak located at the nutrient source. Let us discretize the space plane into a grid, and assume that each state of the Markov chain represents a cell of the grid. To keep things simple, let us also assume that the area where the particle can move is delimited by a square barrier, so that the number of grid cells (which is also the number of states) can be considered finite. Since the probability of transitioning from a state $j$ to a state $k$ depends on the direction the particle had when entering $j$, the natural representation of the setup is by a second order Markov Chain. In other terms, it is intuitive to define the transition probability $P(i, j, k)$ of being at state $k$ at time $t + 1$ if the state at time $t$ is $j$ and the state at time $t - 1$ is $i$. These transition probabilities can be readily computed from the behavioral rule equation. Particular care must be taken when the state $i$ is on the boundary, i.e. when it corresponds to a cell next to the barrier. In this case, we assume that if the particle tries to overcome the barrier, it simply remains in the same state.

More formally, to define a Markov model of the setup, let us assume the Gaussian to be centered at the origin of a 2D Cartesian system, $A(\boldsymbol{x}) = \exp(-\boldsymbol{x}^T \Sigma \boldsymbol{x})$ and consider the region of the first quadrant defined by $0 \leq x_1 \leq D$, $0 \leq x_2 \leq D$, $D \in \mathbb{R}$. Let us discretize this region in $N$ square areas of side $D/N^{1/2}$, and model each region by a state. Fig.5 presents a schematic representation of the Markov model.

Let us then approximate the behavior of Eq. 1 as transitions between

the states placed on this discrete grid. In particular, let us denote by $x^{(i)}$ the ideal location of state $i$ on the plane. The transition probability from a certain state $j$ to a state $k \neq j$ is assumed to be non zero only for the Moore neighbors[1], i.e. the states with Chebyshev distance 1, $\left\|\boldsymbol{x}^{(j)} - \boldsymbol{x}^{(k)}\right\|_\infty = 1$. Let us denote by $F$ the set of the states of the boundary, i.e. the ones for which one of the coordinates of the ideal location is 0 or $D$. The transition from a state to itself is considered to be zero for all the states that do not lie on the boundary. For the states in $F$, the probability of the self transition is set to the sum of the transition probabilities to states that would lie outside the considered region. Let us finally define $M^{(j)}$ as the number of states (inside the region) that are Moore neighbors of $j$, which is 8 for $j \notin F$. With these assumptions, the probability of the transition from a state $i$ to a state $j$ and the subsequent transition to a state $k$ can be approximated by

$$P(i,j,k) = \begin{cases} \int_{a-\pi/8}^{a+\pi/8} f(\theta)d\theta & if j \neq k \wedge i \neq j \wedge A(x^{(i)}) \geq A(x^{(j)}) \\ \frac{1}{M^{(j)}} & if j \neq k \wedge \left(i = j \vee A(x^{(i)}) < A(x^{(j)})\right) \\ \frac{1}{8-M^{(j)}} & if j = k \wedge j \in F \\ 0 & otherwise \end{cases}$$

where $a = \arccos((\boldsymbol{x}^{(j)} - \boldsymbol{x}^{(i)}) \cdot (\boldsymbol{x}^{(k)} - \boldsymbol{x}^{(j)}))$ and again $f(\theta)$ is the Von Mises distribution centered in 0 ($\mu = 0$). The evolution of the distribution over 200 steps was computed for $\kappa = 1/\eta^2 = 0.033$. $N = 400$ states were used to ideally represent square locations set at $[0.5 + p, 0.5 + q]$, $0 \leq p < 20, 0 \leq q < 20,\ p, q \in \mathbb{N}$. The initial distribution was set to simulate all particles in the top right corner, i.e. denoting by $c$ the state on the top-right corner ($x^{(c)} = [19.5, 19.5]^T$) the initial probability was set to $P(c, c) = 1$ and $P(i, j) = 0\ \forall i \neq c \vee j \neq c$.

In order to study the effect of the potential field $A$ on the movement of the particles the calculation was performed using two different Gaussian potential fields. In particular, we tested two setups $A(\boldsymbol{x}) = \exp\left(-\boldsymbol{x}^T \Sigma \boldsymbol{x}\right)$

[1]The model ignores that not all the 8 Moore neighbors are at the same Euclidean distance, i.e. that the ones placed diagonally have a distance $\sqrt{2}$ times bigger. The model can be refined by imagining the states located on an hexagonal grid. Since the results are essentially the same, we chose to present the simplest model.

with $\Sigma = \Sigma_1 = \begin{bmatrix} 1.5 & 0 \\ 0 & 1.5 \end{bmatrix}$ and $\Sigma = \Sigma_2 = \begin{bmatrix} 4 & 0 \\ 1 & 1.5 \end{bmatrix}$, respectively.

Figure 6 reports the results. Expressly, the expected value for the position of the particles $\bar{\boldsymbol{x}}_t = \sum_k \boldsymbol{x}^{(k)} \sum_i \sum_j P(i,j,k)$ at each time step was calculated and highlighted in the two panels. For clarity, the panels also reports contour lines of the potential fields as well as the trajectory obtained joining the ideal location of the expected positions. It clearly appears that the expected trajectory is an approximations of the trajectory obtained by following the steepest gradient. This suggests us that with continuous potential fields, with sufficiently small steps, the behavioral rule of Eq. 1 should be able generate trajectories that approximate the gradient descent, even if the only information used by the algorithm is a binary temporal derivative. Obviously further investigations are necessary to prove the generality of this result.

## 4. Mutual Information

As stated in the introduction, the SR effect reported for the behavioral rule examined in this paper can also be observed by computing the mutual information between the potential field and the spatial distribution of particles that move according to of Eq. 1.

Expressly, let us imagine to have the two Gaussian potential fields presented in the previous section. Again, let us subdivide the region of the first quadrant defined by $0 \leq x_1 \leq D$, $0 \leq x_2 \leq D$, $D \in \mathbb{R}$, in $N$ square subregions of side $D/N^{1/2}$, and for each subregion $i$ let us denote by $x^{(i)}$ the coordinates of its center. Assume the potential field values to be quantized uniformly in $Q_A$ levels. Denote by $\bar{A}(x^{(i)})$ the quantized value of the potential field at $x^{(i)}$. Let us define $P_A(\alpha)$ as the probability that $\bar{A}(x^{(i)})$ is $\alpha$ when the state $i$ is chosen uniformly among the subregions. Clearly $P_A(\alpha) = \left|\{i : \bar{A}(x^{(i)}) = \alpha\}\right| / N$, where $\left|\{i : \bar{A}(x^{(i)}) = \alpha\}\right|$ is the number of subregions for which the quantized value of the potential value in the center is $\alpha$ .

Imagine then to have particles that, as in the previous section, start in the top right corner of the region and move over the potential field according to Eq. 1. The spatial distribution of the particles among the $N$ square areas is intuitively correlated to the potential value. In particular, let us assume to denote by $P_{t,i}$ the probability of a particle being in the subregion $i$ at the $t$-th time step. As done for the potential field values, for simplicity let us quantize evenly these probability values over $Q_C$ levels, and denote by $\bar{P}_{t,i}$ this

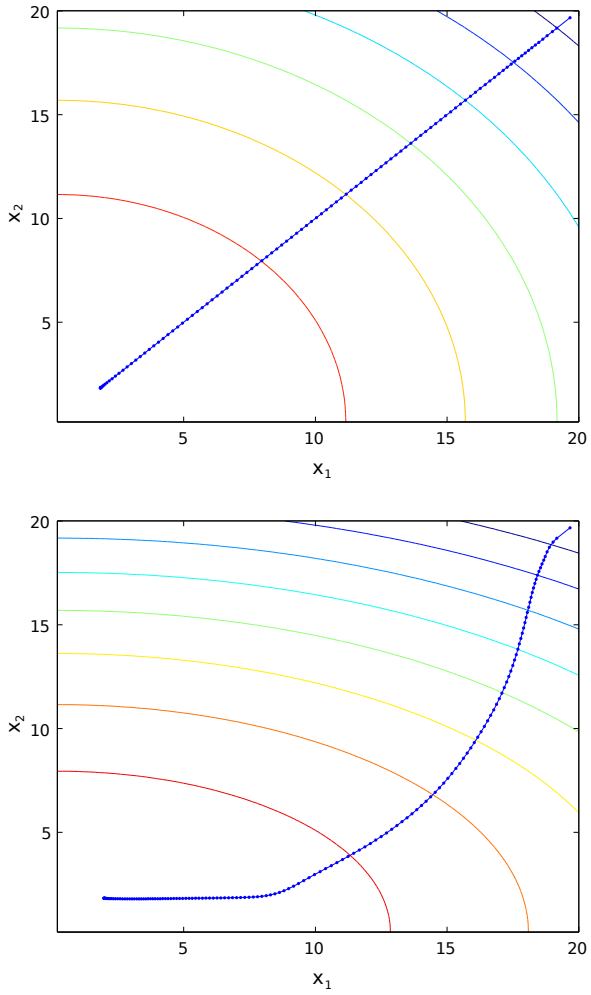


Figure 6: Results of the second order Markov models that represent Gaussian potential fields. The first panel reports the results for $\Sigma_1 = \begin{bmatrix} 1.5 & 0 \\ 0 & 1.5 \end{bmatrix}$ and the second one refers to $\Sigma_2 = \begin{bmatrix} 4 & 0 \\ 1 & 1.5 \end{bmatrix}$. The expected location of the particles at different steps of the Markov chain are reported by blue dots, connected together by a blue line for clarity. Contour lines of the potential field are reported as well. The expected values of the positions taken over time by the particle approximate the steepest gradient in both cases.

quantized values. Similarly to what previously done, let us denote by $P_{t,C}(\gamma)$ the probability that the quantized value of $P_{t,i}$ is $\gamma$ when $i$ is chosen uniformly among the subregions. Finally, let us denote by $P_t(\alpha, \gamma)$ the probability that $A(x^{(i)}) = \alpha$ and $P_{t,i} = \gamma$ when a subregion $i$ is chosen uniformly among the subregions. Given these definitions, the mutual information between the potential field and the spatial distributions of the particles can be expressed as

$$I_t = \sum_{\alpha} \sum_{\gamma} P_t(\alpha, \gamma) \cdot \log_2 \left( \frac{P_t(\alpha, \gamma)}{P_A(\alpha) P_{t,C}(\gamma)} \right)$$

Using the second order Markov Model presented in the previous section it is possible to readily obtain quantitative results on the relationship between the noise level $\eta$ and the mutual information defined here. However memory constraints would impose a very coarse subdivision of the regions for any trivial implementation of the chain. We therefore chose to estimate the probabilities using a Monte Carlo simulation. In particular, the particles were assumed to start at $x^{(c)} = [19.5, 19.5]^T$ and to move by the vector $\boldsymbol{u}_t \in \mathbb{R}^2$, where the vector is selected using Eq. 1 and subsequently normalized as $\boldsymbol{u}_t / \|\boldsymbol{u}_t\|$.

Results were obtained by simulating $10^4$ particles and observing their distribution over $N = 100 \times 100 = 10^4$ subregions at time $t = 35$. The discretizations were performed into $Q_A = Q_c = 100$ levels. Figure 7 reports the mutual information obtained for the two Gaussian potential fields under different magnitudes of the perturbation level. The mutual information curves clearly exhibit a SR effect, with a peak located at approximately $\eta = 0.24$ for the first potential field and $\eta = 0.2$ for the second one.

Once more we find a quantitative confirmation that an opportune level of random perturbation increases the performance of our minimalistic behavioral rule. This increase can be conceptually thought as an increase in the ability of estimating the shape of the potential field from the knowledge of the temporal derivative. The generality of the results will be shown in future works, for instance by the computation of the relationship between random perturbation and mutual information of particle that move over more complex potential fields.

## 5. Conclusion

In this paper, we suggested the possibility that chemotaxis, which is a primitive and essential behavior found in bacteria, could actually be exploit-

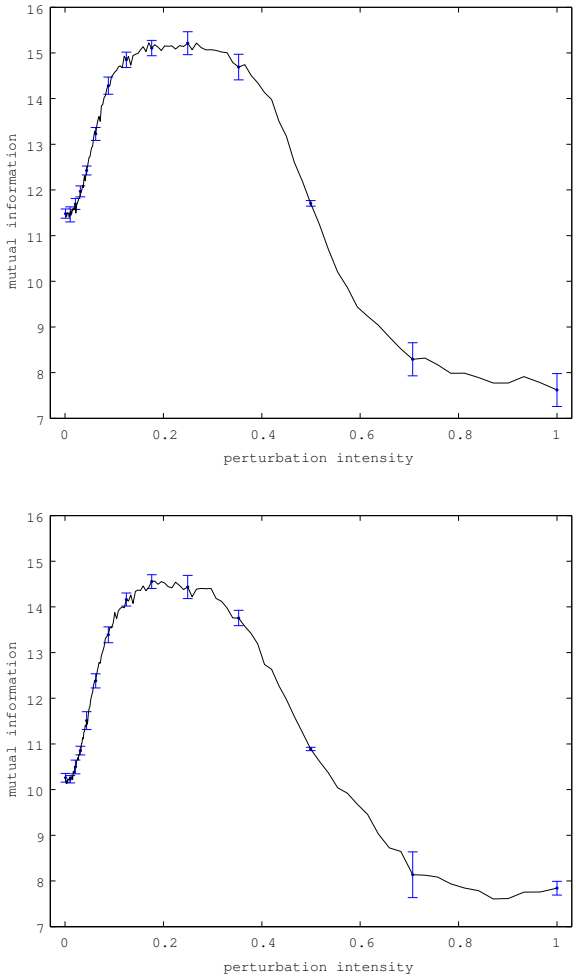


Figure 7: Mutual information for different values of $\eta$. The top panel reports the results for $\Sigma_1 = \begin{bmatrix} 1.5 & 0 \\ 0 & 1.5 \end{bmatrix}$ and the bottom one for $\Sigma_2 = \begin{bmatrix} 4 & 0 \\ 1 & 1.5 \end{bmatrix}$. For some perturbation levels an error bar is used to indicate the standard deviation, estimated by repeating the experiment 10 times.

ing stochastic resonance, and not just be a behavior robust to noise. In order to support this hypothesis, the paper proposes a very simple behavioral rule that could be used to model the chemotactic behavior at a very abstract level. Results show that the application of this rule presents a stochastic resonant behavior, i.e. the addition of a random perturbation of opportune magnitude can improve the performances. Statistical models for the movement of particles according to this rule over simple potential fields were presented. In particular a linearly increasing potential field and Gaussian potential fields were taken into consideration.

More specifically, we showed that particles moving according to our behavioral rule move toward increasing potential values although the only information taken as input is the sign of the temporal difference in the potential value. We showed that the performance can be enhanced by random perturbations of adequate magnitude. A Markov chain model that explains this performance increase in terms of a change of the probability density function of the directions taken by the particles was presented. Furthermore it was suggested by two simple examples that the expected value of the trajectory taken by our algorithm could actually correspond to the steepest gradient.

The SR was studied from the point of view of mutual information between the potential field and the spatial distribution of particles that move according to the proposed behavioral rule. Results showed that, as expected, the mutual information increases for an opportune random perturbation magnitude.

The modeling of chemotaxis provided by our rule is very abstract and far from the complexity of chemical reactions arising in real diffusion of nutrients and their sensing in bacteria. We cannot therefore claim with certainty that SR is exploited in chemotaxis, although the results here presented seem to suggest this possibility.

Future works will need to generalize the results presented in this paper. In particular, in section 3.1 it was highlighted that choosing the following direction completely randomly as soon as the potential decreases even slightly yields higher performances than increasing smoothly the perturbation magnitude as the temporal derivative of the potential fields becomes more strongly negative. Providing a formal proof and identifying the conditions for the optimality of the current choice appears to be a very interesting topic. Similarly, it appears worth investigating the possibility of deriving analytically the conditions for which the expected values of the trajectory generated by the behavioral rule coincides with the steepest gradient trajectories when the

length of the steps tends to 0. Finally, one interesting point to tackle is to analyze whether the performance increase observed can be explained solely by an increase of the sensitivity of the temporal derivative used by the algorithm, or if the SR effect observed is of a type fundamentally different from the SR observed in sensors with thresholds.

The results of this paper show natural applicability in the robotics field as well. In fact, the behavioral rule presented in the paper constitutes an extremely simple adaptive behavioral rule that is applicable in a great variety of setups thanks to the limited information required by the algorithm. The minimal requirements of the rule suggest the possibility of using it as a bootstrap algorithm for more advanced learning methods. Indeed, many learning algorithms require knowledge on the structure of the sensory information, and using this behavioral rule to acquire such knowledge appears as an interesting possibility that will be analyzed in future works.

## References


[1] R. Benzi, A. Sutera, A. Vulpiani, The mechanism of stochastic resonance, Journal of Physics A: mathematical and general 14 (1981) 453–457.

[2] R. Benzi, G. Parisi, A. Sutera, A. Vulpiani, Stochastic resonance in climatic change, Tellus 34 (1982) 10–16.

[3] L. Gammaitoni, P. Hänggi, P. Jung, F. Marchesoni, Stochastic resonance, Reviews of Modern Physics 70 (1) (1998) 223–287.

[4] K. Wiesenfeld, F. Moss, Stochastic resonance and the benefits of noise: from ice ages to crayfish and SQUIDs, Nature 373 (6509) (1995) 33–36.

[5] S. Fauve, F. Heslot, Stochastic resonance in a bistable system, Physics Letters A 97 (1983) 5–7.

[6] B. McNamara, K. Wiesenfeld, R. Roy, Observation of stochastic resonance in a ring laser, Phys. Rev. Lett. 60 (25) (1988) 2626–2629. doi:10.1103/PhysRevLett.60.2626.

[7] R. N. Mantegna, B. Spagnolo, Stochastic resonance in a tunnel diode, Phys. Rev. E 49 (3) (1994) R1792–R1795. doi:10.1103/PhysRevE.49.R1792.

[8] B. Mereu, C. P. Cristescu, M. Alexe, Chaos supported stochastic resonance in a metal-ferroelectric-semiconductor heterostructure., Phys Rev E Stat Nonlin Soft Matter Phys 71 (4 Pt 2) (2005) 047201.

[9] W. Hohmann, J. Müller, F. W. Schneider, Stochastic resonance in chemistry. 3. the minimal-bromate reaction, Journal of Physical Chemistry A 100 (1996) 5388+.

[10] T. Amemiya, T. Ohmori, M. Nakaiwa, T. Yamamoto, T. Yamaguchi, Modeling of nonlinear chemical reaction systems and two-parameter stochastic resonance, Journal of Biological Physics 25 (2-3) (1999) 73–85.

[11] Z. X. Pi, H. W. Xin, Two-parameter stochastic resonance in a model of electrodissolution of fe in $H_2SO_4$, Chinese Chemical Letters 12 (2001) 223–226.

[12] S. Bezrukov, I. Vodyanoy, Stochastic resonance in non-dynamical systems without response thresholds, Nature 385 (6614) (1997) 319–321.

[13] A. Hibbs, A. Singsaas, E. Jacobs, A. Bulsara, J. Bekkedahl, F. Moss, Stochastic resonance in a superconducting loop with a Josephson junction, Journal of Applied Physics 77 (6) (1995) 2582–2590.

[14] F. Mueller, S. Heugel, L. J. Wang, Optomechanical stochastic resonance in a macroscopic torsion oscillator, Phys. Rev. A 79 (3) (2009) 031804. doi:10.1103/PhysRevA.79.031804.

[15] J. Collins, C. Chow, T. Imhoff, Stochastic resonance without tuning, Nature 376 (6537) (1995) 236–238.

[16] S. M. Bezrukov, I. Vodyanoy, Noise-induced enhancement of signal transduction across voltage-dependent ion channels, Nature 378 (6555) (1995) 362–364.

[17] J. Douglass, L. Wilkens, E. Pantazelou, F. Moss, Noise enhancement of information transfer in crayfish mechanoreceptors by stochastic resonance, Nature 365 (6444) (1993) 337–340.

[18] J. Levin, J. Miller, Broadband neural encoding in the cricket cercal sensory system enhanced by stochastic resonance, Nature 380 (1996) 165–168.

[19] B. J. Gluckman, T. I. Netoff, E. J. Neel, W. L. Ditto, M. L. Spano, S. J. Schiff, Stochastic resonance in a neuronal network from mammalian brain, Phys. Rev. Lett. 77 (19) (1996) 4098–4101. doi:10.1103/PhysRevLett.77.4098.

[20] P. Cordo, J. T. Inglis, S. Verschueren, J. J. Collins, D. M. Merfeld, S. Rosenblum, S. Buckley, F. Moss, Noise in human muscle spindles, Nature 383 (6603) (1996) 769–770.

[21] J. J. Collins, T. T. Imhoff, P. Grigg, Noise-enhanced tactile sensation, Nature 383 (6603) (1996) 770.

[22] L. Chen, R. Wang, T. Zhou, K. Aihara, Noise-induced cooperative behavior in a multicell system, Bioinformatics 21 (11) (2005) 2722–2729. doi:http://dx.doi.org/10.1093/bioinformatics/bti392.

[23] D. Russell, L. Wilkens, F. Moss, Use of behavioural stochastic resonance by paddle fish for feeding, Nature 402 (6759) (1999) 291–294.

[24] A. Priplata, B. Patritti, J. Niemi, R. Hughes, D. Gravelle, L. Lipsitz, A. Veves, J. Stein, P. Bonato, J. Collins, Noise-enhanced balance control in patients with diabetes and patients with stroke., Ann Neurol 59 (1) (2006) 4–12.

[25] K. Kitajo, K. Yamanaka, L. M. Ward, Y. Yamamoto, Stochastic resonance in attention control, EPL (Europhysics Letters) 76 (6) (2006) 1029.

[26] J. Adler, The sensing of chemicals by bacteria, Scientific American 234 (1976) 40–47.

[27] J. E. Segall, S. M. Block, H. C. Berg, Temporal comparisons in bacterial chemotaxis, Proceedings of the National Academy of Sciences of the United States of America 83 (23) (1986) 8987–8991.

[28] C. V. Rao, J. R. Kirby, A. P. Arkin, Design and diversity in bacterial chemotaxis: A comparative study in escherichia coli and bacillus subtilis, PLoS Biol 2 (2) (2004) e49. doi:10.1371/journal.pbio.0020049.

[29] S. Zigmond, Mechanisms of sensing chemical gradients by polymorphonuclear leukocytes, Nature (1974) 450–452.

[30] P. Devreotes, S. Zigmond, Chemotaxis in eukaryotic cells: a focus on leukocytes and Dictyostelium, Annual review of cell biology 4 (1) (1988) 649–686.

[31] C. Parent, P. Devreotes, A cell's sense of direction, Science 284 (5415) (1999) 765.

[32] C. Parent, Making all the right moves: chemotaxis in neutrophils and Dictyostelium, Current opinion in cell biology 16 (1) (2004) 4–13.

[33] P. Van Haastert, P. Devreotes, Chemotaxis: signalling the way forward, Nature Reviews Molecular Cell Biology 5 (8) (2004) 626–634.

[34] P. R. Patnaik, A feasibility analysis of bacterial chemotaxis under the influence of external noise, Journal of Biochemical Technology 2 (2009) 119–125.

[35] M. J. Schnitzer, Theory of continuum random walks and application to chemotaxis, Phys. Rev. E 48 (4) (1993) 2553–2568. doi:10.1103/PhysRevE.48.2553.

[36] M. D. Baker, P. M. Wolanin, J. B. Stock, Systems biology of bacterial chemotaxis, Current Opinion in Microbiology 9 (2) (2006) 187 – 192, cell Regulation / Edited by Werner Goebel and Stephen Lory. doi:DOI: 10.1016/j.mib.2006.02.007.

[37] L. Jiang, Q. Ouyang, Y. Tu, Quantitative modeling of escherichia coli chemotactic motion in environments varying in space and time, PLoS Comput Biol 6 (4) (2010) e1000735. doi:10.1371/journal.pcbi.1000735.

[38] B. W. Andrews, T.-M. Yi, P. A. Iglesias, Optimal noise filtering in the chemotactic response of escherichia coli, PLoS Comput Biol 2 (11) (2006) e154. doi:10.1371/journal.pcbi.0020154.

[39] K. Shirai, Y. Matsumoto, Y. Nakamura, S. Koizumi, H. Ishiguro, Noise-based underactuated mobile robot inspired by bacterial motion mechanism, in: Proceedings of the 2009 IEEE/RSJ international conference on Intelligent robots and systems, IEEE Press, 2009, pp. 1043–1048.

[40] S. Nurzaman, Y. Matsumoto, Y. Nakamura, S. Koizumi, H. Ishiguro, Yuragi-based adaptive searching behavior in mobile robot: From bacterial chemotaxis to levy walk, in: IEEE International Conference on Robotics and Biomimetics 2008, ROBIO 2008, 2009, pp. 806 – 811.

[41] I. Fukuyori, Y. Nakamura, Y. Matsumoto, H. Ishiguro, Flexible control mechanism for multi-dof robotic arm based on biological fluctuation, From Animals to Animats 10 (2010) 22–31.

[42] Y. Ishii, Y. Taniguchi, M. Iwaki, T. Yanagida, Thermal fluctuations biased for directional motion in molecular motors, Biosystems 93 (1-2) (2008) 34 – 38. doi:DOI: 10.1016/j.biosystems.2008.04.015.

[43] A. Dhariwal, G. S. Sukhatme, A. A. G. Requicha, Bacterium-inspired robots for environmental monitoring, in: 2004 IEEE International Conference on Robotics and Automation (ICRA 2004), New Orleans, USA, 2004, pp. 1436–1443.

[44] F. DallaLibera, S. Ikemoto, T. Minato, H. Ishiguro, E. Menegatti, E. Pagello, Biologically inspired mobile robot control robust to hardware failures and sensor noise, in: RoboCup Symposium 2010, 2010.

[45] F. DallaLibera, S. Ikemoto, T. Minato, H. Ishiguro, E. Menegatti, E. Pagello, A parameterless biologically inspired control algorithm robust to nonlinearities, dead-times and low-pass filtering effects, in: Simulation, Modeling, and Programming for Autonomous Robots (SIMPAR 2010), Vol. 6472, Darmstadt, Germany, 2010, p. 362373.